Hbxip is essential for embryogenesis and regulates embryonic stem cell differentiation through activating mTORC1

Yan Qin[1,2], Peiling Ni[1,2], Qingye Zhang[1], Xiao Wang[1], Xiaoling Du[1], Zixi Yin[1], Lingling Wang[1], Lihong Ye[1,*], Lingyi Chen[1,*]

[1] Institute of Translational Medicine, Tianjin Union Medical Center, State Key Laboratory of Medicinal Chemical Biology, Tianjin Key Laboratory of Protein Sciences, Frontiers Science Center for Cell Responses, National Demonstration Center for Experimental Biology Education and College of Life Sciences, Nankai University, Tianjin, China

[2] These authors contributed equally.

[*] Correspondence: Lingyi Chen, lingyichen@nankai.edu.cn;
Lihong Ye, yelihong@nankai.edu.cn.

Key words: Hbxip, Lamtor5, embryogenesis, embryonic stem cells, mTORC1.

SUMMARY STATEMENT

Qin et al. characterized the essential role of Hbxip in embryogenesis and embryonic stem cell differentiation, and demonstrated that Hbxip is required for activating mTORC1 in these processes.

ABSTRACT

Hbxip, also named Lamtor5, has been well characterized as a transcriptional coactivator in various cancers. However, the role of Hbxip in normal development remains unexplored. Here, we demonstrated that homozygous knockout of *Hbxip* leads to embryonic lethality, with retarded growth around E7.5, and that depletion of Hbxip compromises the self-renewal of embryonic stem cells (ESCs), with reduced expression of pluripotency genes, reduced cell proliferation, and decreased colony forming capacity. In addition, both *Hbxip*$^{-/-}$ ESCs and E7.5 embryos display defects in ectodermal and mesodermal differentiation. Mechanistically, Hbxip interacts with

other components of the Ragulator complex, which is required for mTORC1 activation by amino acids. Importantly, ESCs depleted of Ragulator subunits, Lamtor3 or Lamtor4, display differentiation defects similar to those of *Hbxip*$^{-/-}$ ESCs. Moreover, *Hbxip*$^{-/-}$, *p14*$^{-/-}$, and *p18*$^{-/-}$ mice, lacking subunits of the Ragulator complex, also share similar phenotypes, embryonic lethality and retarded growth around E7-8. Thus, we conclude that Hbxip plays a pivotal role in the development and differentiation of the epiblast, as well as the self-renewal and differentiation of ESCs, through activating mTORC1 signaling.

INTRODUCTION

Hepatitis B X-interacting protein (HBXIP, also known as LAMTOR5), was first identified as a binding factor to Hepatitis B virus X protein (Melegari et al., 1998). In addition to its role in inhibiting the replication of Hepatitis B virus, HBXIP has been extensively studied in various cancers. It has been shown that HBXIP promotes proliferation, migration and tumorigenesis of breast, ovarian, liver, non-small-cell lung, bladder urothelial, and esophageal squamous cell cancer (Hu et al., 2011, Liu et al., 2012, Liu et al., 2014, Xu et al., 2014, Zhang et al., 2014, Li and Liu, 2016, Shi et al., 2016, Wang et al., 2017b, Zhou et al., 2019b, Wu et al., 2020). Overexpression of HBXIP is associated with poor prognosis in breast, ovarian, liver, non-small-cell lung cancer and pancreatic ductal adenocarcinomas (Wang et al., 2017b, Li et al., 2017, Wang et al., 2017c, Zhou et al., 2019a, Cheng et al., 2014). HBXIP also contributes to cisplatin and tamoxifen resistance in ovarian and breast cancers, respectively (Zou et al., 2017, Liu et al., 2018). However, the role of HBXIP in normal development remains poorly understood. Only a recent work reported that due to the pivotal role of Hbxip in activating the transcription of insulin by elevating the level of Pdx-1/Neurod1 complex, pancreatic β-cell-specific *Hbxip* knockout (KO) mice display higher fasting blood glucose levels and impaired glucose tolerance (Li et al., 2018).

The extensive studies of HBXIP in cancers have revealed its function as a transcriptional cofactor. HBXIP, cooperating with various transcription factors, such as c-MYB, SP1, cAMP response element-binding protein (CREB), TATA-binding protein (TBP), and E2F1, activates the expression of its downstream target genes, including *YAP*, *FGF8*, *LIN28B*, *SKP2*, *PDGFB*, *S100A4*, and *LMO4*, consequently promoting proliferation and migration of cancer cells (Liu et al., 2012, Liu et al., 2014, Xu et al., 2014, Liu et al., 2013, Xu et al., 2013, Yue et al., 2013,

Zhang et al., 2013, Wang et al., 2017a). In addition, HBXIP may interact with proteins other than transcription factors to fulfill its biological functions. HBXIP interacts with survivin to suppress caspase activation and hence apoptosis (Marusawa et al., 2003). HBXIP also associates with microtubules and centrosomes in dividing cells, and is required for the proper formation of centrosomes and spindles in HeLa cells (Wen et al., 2008, Fujii et al., 2006). Moreover, HBXIP, together with p18 (LAMTOR1), p14 (LAMTOR2), MP1 (LAMTOR3) and C7ORF59 (LAMTOR4), form a pentameric Ragulator complex, which is required for mTORC1 activation by amino acids (Bar-Peled et al., 2012). Yet, whether HBXIP regulates normal development or carcinogenesis through the mTORC1 pathway remains unexplored.

In this study, we demonstrated that KO of *Hbxip* is embryonic lethal, and retarded development of *Hbxip*$^{-/-}$ embryos become obvious around E7.5. Using *Hbxip* KO embryonic stem cells (ESCs) as an *in vitro* model, we found that *Hbxip* is critical for the differentiation of ESCs, particularly for the ectodermal and mesodermal differentiation. Consistently, the epiblast of E8.5 *Hbxip*$^{-/-}$ embryos remains undifferentiated. The differentiation defects are shared by ESCs lacking subunits of the Ragulator complex, including Hbxip, Lamtor3, and Lamtor4. Thus, we concluded that Hbxip regulates embryo development and ESC differentiation through activating the mTORC1 signaling.

RESULTS

Embryonic lethality in *Hbxip* null embryos

To study the function of Hbxip in normal development, we knocked out *Hbxip* in previous generated *Hbxip* floxed mice (Fig. 1A) (Li et al., 2018). Heterozygous *Hbxip* KO (*Hbxip*$^{+/-}$) mice were obtained through mating between *Hbxip* floxed mice and *EIIa-cre* mice. *Hbxip*$^{+/-}$ mice are fertile. Yet, no *Hbxip*$^{-/-}$ mice were born from *Hbxip*$^{+/-}$ intercrosses (Fig. 1C), indicating embryonic lethality of *Hbxip* null mice. To determine the timing of lethality, E3.5, E6.5, E7.5 and E9.5 embryos from *Hbxip*$^{+/-}$ intercrosses were genotyped, and *Hbxip*$^{-/-}$ embryos were detected at all the analyzed time points (Fig. 1C). However, at 7.5 days postcoitum, *Hbxip*$^{-/-}$ embryos are smaller than WT and *Hbxip*$^{+/-}$ embryos (Fig. 1D, E). At 8.5 and 9.5 days postcoitum, *Hbxip*$^{-/-}$ embryos appear to be developmentally arrested, compared to their WT and *Hbxip*$^{+/-}$ littermates (Fig. 1D). These data suggest a critical role of Hbxip in embryonic development.

Hbxip KO compromises the self-renewal of embryonic stem cells

Next, we utilized *in vitro* cultured mouse embryonic stem cells (ESCs) to understand the mechanism of Hbxip in embryonic development. *Hbxip* KO ESC lines were constructed using CRISPR/Cas9, with a sgRNA targeting to the third exon of *Hbxip* (Fig. 2A). The disruption of *Hbxip* in two independent ESC clones (hereafter referred to as $H^{-/-}$*-1* and $H^{-/-}$*-2*) with normal karyotype was validated by loss of the *Ban* I site, Sanger sequencing, and Western Blot (Figs 2A, B, S1A-D). Notably, deletion of *Hbxip* compromises the self-renewal of ESCs, demonstrated by reduced proliferation rate and colony-forming capacity (Fig. 2C, D). But *Hbxip* KO does not change the cell cycle profile or induce apoptosis in ESCs (Fig. S1E, F). The mRNA levels of pluripotency genes, *Nanog*, *Oct4*, and *Sox2*, as well as the protein levels of Nanog and Oct4, are declined in *Hbxip* KO ESCs (Fig. 2B, E). In addition, in undifferentiated ESCs, *Hbxip* KO suppresses the expression of ectodermal, and mesodermal markers, such as *Nestin*, *Celsr2*, *T*, and *Dlx3*, whereas endodermal marker *Gata6* is activated by *Hbxip* KO (Fig. 2F). All these data suggest an essential role of *Hbxip* in ESC self-renewal.

Transcriptomic analysis identified 787 upregulated genes and 1494 downregulated genes shared by $H^{-/-}$*-1* and $H^{-/-}$*-2* ESCs, compared to WT ESCs (Fig. 2G and Table S2). Gene ontology (GO) annotation revealed that several developmental terms, such as system development, nervous system development and ectoderm development, are enriched in the downregulated genes (Figs 2H, S2A). These data imply that Hbxip might be involved in ESC and epiblast differentiation.

Hbxip KO causes differentiation defects in ESCs

We then tested the role of Hbxip in the differentiation of ESCs. Two methods were used to differentiate ESCs, either by LIF withdrawal or by embryoid body (EB) formation in hanging drops. Under these two differentiation conditions, $Hbxip^{-/-}$ ESCs fail to activate differentiation genes, including ectodermal markers, *Nestin* and *Celsr2*, and mesodermal markers, *T* and *Dlx3* (Fig. 3A, B). Through RNA-seq analysis, 1028 downregulated genes and 482 upregulated genes are identified in differentiated $Hbxip^{-/-}$ cells induced by LIF withdrawal, compared to differentiated WT cells (Fig. 3C), while *Hbxip* KO downregulates 719 genes and upregulates 655 genes in day 4 EBs (Fig. 3D and Table S3). Differentiated $Hbxip^{-/-}$ cells by LIF withdrawal and day 4 $Hbxip^{-/-}$ EBs share 481 downregulated genes and 325 upregulated genes (Fig. 3E and Table

S3). GO analysis revealed that genes involved in system development, mesoderm development, ectoderm development, embryo development and cell differentiation are enriched in the downregulated genes (Figs 3F, S2B).

To further confirm the roles of *Hbxip* in pluripotency maintenance and ESC differentiation, rescue experiments were performed in $H^{-/-}$*-1* ESCs by expressing either short isoform (H-S) or long isoform (H-L) of *Hbxip*. Both H-S and H-L rescue the expression levels of Nanog and Oct4 proteins in undifferentiated ESCs (Figs 3G, S2C), as well as the expression of differentiation genes, *Nestin*, *Celsr2*, *T*, and *Dlx3*, in differentiated cells (Fig. 3H). These data indicate that Hbxip is required for the proper differentiation of ESCs, particularly toward the ectodermal and mesodermal lineages.

Hbxip$^{-/-}$ embryos are defective in epiblast formation and differentiation

Given the differentiation defects of *Hbxip*$^{-/-}$ ESCs, we tested whether the epiblast properly differentiates into three germ layers, particularly the ectoderm and mesoderm. Immunohistochemistry staining with Hbxip antibody allowed us to distinguish *Hbxip*$^{-/-}$ embryos from WT and *Hbxip*$^{+/-}$ embryos (Fig. 4). Hematoxylin-eosin (H&E) staining showed that the development of amnion cavity is retarded in E7.5 *Hbxip*$^{-/-}$ embryos (Fig. 4A). Immunofluorescent staining of Oct4 demonstrated that the epiblast in E7.5 *Hbxip*$^{-/-}$ embryos is much smaller than that in E7.5 WT and *Hbxip*$^{+/-}$ embryos, indicating defective epiblast formation (Fig. 4A). At 8.5 days postcoitum, the morphology of WT and *Hbxip*$^{+/-}$ embryos changes drastically as the initiation of somitogenesis. In contrast, the development of *Hbxip*$^{-/-}$ embryos does not progress further. Importantly, with the formation of three germ layers, Oct4 expression is diminished in E8.5 WT and *Hbxip*$^{+/-}$ embryos, whereas *Hbxip*$^{-/-}$ embryos retain Oct4 expression in the epiblast (Fig. 4B). We further examined the expression of germ layer markers in E7.5 embryos, and found that ectodermal marker Nestin and mesodermal marker T are not expressed in E7.5 *Hbxip*$^{-/-}$ embryos, while the expression of endodermal marker Gata4 is not affected by *Hbxip* KO (Fig. 4C). Taken together, these results suggest that *Hbxip*$^{-/-}$ embryo lethality is due to the defects in epiblast proliferation, ectodermal and mesodermal differentiation.

Hbxip is required for the activation of mTORC1

Next, we investigated the molecular mechanism of Hbxip in embryonic development and ESC differentiation. It has been shown that HBXIP functions as a transcriptional cofactor in many cancers (Liu et al., 2012, Liu et al., 2014, Xu et al., 2014, Liu et al., 2013, Xu et al., 2013, Yue et al., 2013, Zhang et al., 2013, Wang et al., 2017a). We first determined the subcellular distribution of Hbxip in ECSs by Western blot with cytoplasmic and nuclear fractions of ESCs. The result showed that Hbxip is almost exclusively distributed in the cytoplasm (Fig. 5A), thus excluding its function as a transcriptional cofactor.

To understand the molecular mechanism of Hbxip, coimmunoprecipitation (co-IP) coupled with mass spectrometric analysis was performed to identify Hbxip interacting proteins. 128 proteins were identified in the H-S and H-L co-IP samples, but not in the control co-IP sample (Fig. 5B and Table S4). GO analysis revealed that these Hbxip interacting proteins are enriched in mTOR signaling, macroautophagy, PI3K cascade, and signaling by insulin receptor (Fig. 5C). It has been shown that HBXIP is a member of the Ragulator complex which recruits mTORC1 to the lysosome, therefore activating the mTORC1 signaling pathway (Bar-Peled et al., 2012). Consistently, three Ragulator components, Lamtor1 (p18), Lamtor2 (p14), and Lamtor3 (MP1), as well as a mTORC1 subunit Rptor, were identified as Hbxip interacting proteins (Fig. 5C and Table S4). Thus, we speculated that mTORC1 is the key downstream factor of Hbxip in ESCs and embryos. To test this hypothesis, we first showed that the activity of mTORC1 is reduced in *Hbxip*$^{-/-}$ ESCs and embryos, as indicated by the level of phosphorylated S6K1 and 4EBP1 (Figs 5D, S3). Next, we tried to reactivate mTORC1 to rescue the differentiation defects of *Hbxip*$^{-/-}$ ESCs. However, even though knockout of *Tsc1*, overexpression of Rheb or Rptor fused with the lysosome-targeting signal of Rheb (R-R15) (Sancak et al., 2010, Duvel et al., 2010, Long et al., 2005), successfully activate mTORC1 in WT ESCs, these strategies failed to activate the mTORC1 signaling in *Hbxip*$^{-/-}$ ESCs (Figs 5E, 5F, S4), demonstrating the essential role of Hbxip in mTORC1 activation.

mTORC1 inactivation accounts for the defects in ESC self-renewal and differentiation

Failure in activating mTORC1 in *Hbxip*$^{-/-}$ ESCs indicates that Hbxip is essential for mTORC1 activation. Yet, it rendered the rescue experiment impossible. To prove that inactivation of mTORC1 is responsible for the self-renewal and differentiation defects in *Hbxip*$^{-/-}$

ESCs, an alternative strategy was applied. Instead of the rescue experiment, we knocked out genes encoding other components of the Ragulator complex, such as *Lamtor3* and *Lamtor4*, in ESCs (Fig. S5). Similar to *Hbxip*$^{-/-}$ ESCs, *Lamtor3*$^{-/-}$ and *Lamtor4*$^{-/-}$ ESCs display self-renewal defects, including reduced protein levels of Oct4 and Nanog, down-regulated *Oct4*, *Nanog*, and *Sox2* mRNA expression, slower proliferation rate, and decreased colony forming capacity (Fig. 6A-D). Moreover, upon differentiation, *Lamtor3*$^{-/-}$ and *Lamtor4*$^{-/-}$ ESCs also fail to activate ectodermal and mesodermal markers (Fig. 6E, F), just as what we observed in *Hbxip*$^{-/-}$ ESCs (Fig. 3A, B). All these data indicate that inactivation of mTORC1 leads to the self-renewal and differentiation defects in ESCs.

DISCUSSION

In this study, we demonstrated that Hbxip is essential for embryonic development and ESC differentiation. *Hbxip*$^{-/-}$ ESCs, as well as *Lamtor3*$^{-/-}$, and *Lamtor4*$^{-/-}$ ESCs, with disrupted Ragulator complex, display differentiation defects toward ectodermal and mesodermal lineages (Figs 3A, 3B, 6E, 6F). Moreover, *Hbxip*$^{-/-}$, *p14*$^{-/-}$, and *p18*$^{-/-}$ mice, lacking subunits of the Ragulator complex, are embryonic lethal, and retarded growth of these embryos are detected at the same developmental stage, around E7-8 (Fig. 1C, D) (Nada et al., 2009, Teis et al., 2006). These data indicate that the phenotypes of *Hbxip*$^{-/-}$ embryos and ESCs are mainly caused by loss function of the Ragulator complex, rather than lacking the transcriptional coactivator role of Hbxip.

The Ragulator complex is required for the activation of mTORC1 by amino acids (Sancak et al., 2010, Bar-Peled et al., 2012). Consistently, the mTORC1 activity is reduced in *Hbxip*$^{-/-}$ ESCs (Figs 5D, S3A). KO of *Tsc1* and overexpression of Rheb or R-R15 fail to activate mTORC1 in the absence of Hbxip (Fig. 5E, F). In addition, the reduced mTORC1 activity by disruption of the Ragulator complex allows us to investigate the function of mTORC1 in post-implantation embryo development. Deletion of mTORC1 components, mTor and Rptor, results in peri-implantation embryonic death around E5.5-6.5 (Gangloff et al., 2004, Murakami et al., 2004, Guertin et al., 2006), thus preventing studying the role of mTORC1 in later stage of embryogenesis. Nevertheless, *Hbxip*$^{-/-}$, *p14*$^{-/-}$, and *p18*$^{-/-}$ embryos, in which mTORC1 activity is presumably attenuated, develop further after implantation, and retarded growth appears around E7-8. The reduced size of E7.5 *Hbxip*$^{-/-}$ embryos might be attributed to slower cell proliferation

rate caused by decreased mTORC1 activity. Moreover, the differentiation defects of *Hbxip*$^{-/-}$ ESCs (Fig. 3A, B) imply that *Hbxip*$^{-/-}$ epiblast might be defective in differentiation. Indeed, the differentiation of *Hbxip*$^{-/-}$ epiblast is compromised, as indicated by the sustained expression of Oct4 in E8.5 *Hbxip*$^{-/-}$ embryos, and the failure in expressing ectodermal marker Nestin and mesodermal marker T in in E7.5 *Hbxip*$^{-/-}$ embryos (Fig. 4), suggesting that mTORC1 activity is pivotal for epiblast differentiation. Consistent with this note, inhibition of mTOR by INK128 induces a paused pluripotent state in the blastocyst, mimicking diapause (Bulut-Karslioglu et al., 2016), further supporting the role of mTORC1 in the exit from pluripotency.

Even though *Hbxip*$^{-/-}$ epiblasts and *Hbxip*$^{-/-}$ ESCs are both defective in activating the expression of ectodermal and mesodermal markers, Oct4 expression is sustained in E8.5 *Hbxip*$^{-/-}$ embryos, while the downregulation of *Oct4* is not affected during the differentiation of *Hbxip*$^{-/-}$ ESCs. It is most likely due to that *in vitro* differentiation of ESCs cannot recapture all the features of *in vivo* embryo development, even though it mimics *in vivo* development of embryos. It is possible that the downregulation of Oct4 in developing embryos might require the activation of differentiation genes, whereas the repression of *Oct4* could be triggered by LIF withdrawal during ESC differentiation, regardless whether differentiation genes are activated or not. Another seemly conflicting point is that differentiation genes are not activated in *Hbxip*$^{-/-}$ ESCs, in which pluripotency genes are downregulated. This is likely due to the unique effect of mTOR inhibition in ESCs. mTOR inhibition induces pausing of ESCs, which display global transcriptional suppression, including both pluripotency genes and differentiation genes (Bulut-Karslioglu et al., 2016). Thus, the reduced mTORC1 activity in *Hbxip*$^{-/-}$ ESCs may be responsible for simultaneous downregulation of pluripotency genes and differentiation genes.

mTOR signaling is involved in growth and disease through regulating gene transcription, mRNA degradation, protein synthesis, autophagy, lipid and carbohydrate metabolism (Giguere, 2018, Villa et al., 2021, Cho et al., 2021, Mossmann et al., 2018, Saxton and Sabatini, 2017). Further studies are required to elucidate how mTORC1 regulated by the Ragulator complex promotes the differentiation of the epiblast and ESCs. *Hbxip*$^{-/-}$, *Lamtor3*$^{-/-}$, and *Lamtor4*$^{-/-}$ ESCs provide an excellent *in vitro* experimental system for mechanistic investigation.

MATERIALS AND METHODS

Mice

Nankai Animal Care and Use Committee approved the use of mice for this research (Approval number: 2021-SYDWLL-000469). *EIIa-cre* mice (Lakso et al., 1996), which express Cre at a very early stage of preimplantation embryogenesis, most likely at the zygote stage, and are useful for whole-body and germ line deletion of floxed allele, were purchased from Shanghai Model Organisms. *Hbxip*$^{-/-}$ mice were obtained by crossing *Hbxip*$^{+/-}$ mice. All mice were maintained in the C57BL/6 background. Genotyping was performed as described previously (Qin et al., 2019). DNA was isolated from dissected embryos or the tail tips of 2-week mice, and then analyzed by PCR. The sequences of primers (illustrated in Fig. 1A) are listed below. F1: 5'-TTTTTGTCACTCTCGCCTTTG-3', R1: 5'-GCTGGTATGTACTCACCCATT-3', F2: 5'-GCTCTATGGCTTCTGAGGCGGAA, R2: 5'-CTCATCCGACAGGGTACCACGG-3'.

Embryo collection

Embryo manipulation experiments were carried out as described previously (Zhou et al., 2018). Female *Hbxip*$^{+/-}$ mice (4-6 weeks) were induced to superovulate by intraperitoneal injection of 5 IU pregnant mare serum gonadotropin (PMSG, Calbiochem) and 48 hours later 5 IU human chorionic gonadotropin (hCG, Sigma). Then females were mated with male *Hbxip*$^{+/-}$ mice overnight. The next morning, females were checked for the presence of a vaginal plug, designed as E0.5. Zygote and E3.5 embryos were flushed from oviducts at day 0.5 or day 3.5 post-hCG. E6.5, E7.5, E8.5 and E9.5 embryos were collected at corresponding time points after successful mating.

Histological analysis

Embryos were dissected from mice immediately after euthanasia, fixed in 4% paraformaldehyde (PFA) for up to 24 h, stored in 70% ethanol and embedded in paraffin. Then 5 μm-thick sections were prepared using rotary microtome (Leica) and mounted on glass slides. After deparaffinization, sections were stained with hematoxylin and eosin (H&E) for histological analysis.

Immunohistochemistry (IHC) analysis

After deparaffinization, sections were boiled in 1× citrate buffer (ORIGENE, ZLI-9064) and then microwaved at low power for 15 minutes. After cooling to room temperature (RT), the sections were blocked with 5% bovine serum albumin (BSA) at RT for 45 minutes, and then incubated with primary antibody (α-Hbxip, CST, 14633S, 1:200) at RT for 1 h. After three washes with 1×PBS buffer and 3% H_2O_2 treatment for 10 minutes, the slides were incubated with goat anti-rabbit IgG conjugated to horseradish peroxidase (HRP) (ORIGENE, ZB-2301) at RT for 1 h. The HRP activity was detected by the Vectastain ABC (avidin-biotin-peroxidase) kit (Vector Laboratories) as recommended by the manufacturer. The slides were examined using a Leica Microscope, and images were captured with a Leica DFC420C camera.

Immunofluorescence (IF) analysis

The IF of paraffin sections was carried out as described previously (Qin et al., 2019). After deparaffinization, the sections were blocked with 5% goat serum at RT for 45 minutes, then incubating with primary antibody (α-Oct4, Abcam, ab181557, 1:200; α-Nestin, absin, abs137231, 1:100; α-Brachyury (T), Abmart, T58977, 1:100; α-Gata4, Abcam, ab84593, 1:200; α-p-S6K1, Sigma, SAB4301518, 1:100) at RT for 1 h. After washing in 1×PBS buffer for three times, the slides were incubated with Alexa Fluor 594 conjugated goat anti-rabbit IgG (Invitrogen, A11037) at RT for 1 h. The nucleus was stained with DAPI (Thermo Fisher). All images were captured with Leica DM3000 microscope with DFC420C camera.

Cell culture and Transfection

Mouse ESCs (E14 and its derivatives) were cultured in high glucose DMEM (GIBCO) supplemented with 15% fetal bovine serum (FBS, Hyclone), 1% penicillin/streptomycin, 1% L-glutamine, 1% β-mercaptoethanol (Sigma), 1% non-essential amino acids (NEAA, Invitrogen) and 1000 U/mL LIF (ESGRO, Chemicon), plated on gelatin-coated tissue culture dish, and grown in a humidified 5% CO_2 at 37℃. Transfection was carried out with Lipofectamine® 3000 (Invitrogen) according to the manufacturer's instruction. For construction of stably transfected clones, puromycin (1.25 μM) selection was applied for 5-7 days, starting from 24 hours after transfection. All ESC lines are routinely tested for mycoplasma contamination.

Vector construction

pX330-U6-Chimeric_BB-CBh-hSpCas9 (pX330) vector was used to construct gene knockout plasmids targeting *Hbxip*, *Tsc1*, *Lamtor3* and *Lamtor4*. sgRNA was designed in Zhang Feng's online website (http://crispr.mit.edu/). A pair of sgRNA oligos containing the guide sequence were annealed and ligated to the *Bbs*I-linearized vector pX330. The sgRNA oligos targeting *Hbxip*: 5'-CACCGTCTCACTATTCTCTAGGCCG-3' and 5'-AAACCGGCCTAGAGAATAGTGAGAC-3'. The sgRNA oligos targeting *Tsc1*: 5'-CACCGGTGGTCAGGATGTGCAATAC-3' and 5'-AAACGTATTGCACATCCTGACCACC-3'. The sgRNA oligos targeting *Lamtor3*: 5'-CACCGTCCTGTACAAAAAGTTGCCA-3' and 5'-AAACTGGCAACTTTTTGTACAGGAC-3'. The sgRNA oligos targeting *Lamtor4*: 5'-CACCGTGTGCTGACCAACTCCGAGA-3' and 5'-AAACTCTCGGAGTTGGTCAGCACAC-3'; 5'-CACCGCTGCTTGCTCATCGTTCTCA-3' and 5'-AAACTGAGAACGATGAGCAAGCAGC-3'.

Cell proliferation assay

1×10^5 ESCs were plated in 12-well plates in triplicates. Cells were passaged continuously, and counted every 2 days.

Western Blotting

ESCs were collected and dissociated in cold lysis buffer (20 mM HEPES, pH 7.7; 5 mM KCl; 1.5 mM $MgCl_2$; 2 mM DTT; 2 mM PMSF) for 30 minutes on ice. Then the cell lysate was centrifuged at 12,000 rpm, 15 minutes at 4 ℃. Protein concentration was measured using BCA Protein Assay Kit (Beyotime). The samples were resolved with SDS-PAGE gel and transferred onto PVDF membrane. Then, the PVDF membrane was incubated in blocking buffer for 1 hour at RT, followed by incubating with primary antibodies (α-Hbxip, CST, 14633S, 1:2000; α-Nanog, Bethyl Laboratories, A300-397A, 1:2000; α-Oct4, Santa Cruz, sc-5279, 1:1000; α-Tubulin, Sigma, ASB4800087, 1:2000; α-S6K1, Sigma, SAB4502686, 1:1000; α-p-S6K1, Sigma, SAB4301518, 1:1000; α-H3, Abcam, ab1791, 1:2000; α-Tsc1, Absin, abs131176, 1:2000; α-MP1/Lamtor3, Novus, NBP1-50631, 1:2000; α-C7orf59/Lamtor4, CST, D4P6O, 1:2000; α-p-4EBP1, CST, 2855, 1:2000; α-4EBP1, CST, 9452, 1:2000) at 4 ℃ overnight. After washing three times, the membrane was incubated with HRP-liked secondary antibodies at RT

for 1 hour. Immunoreactivity was detected by ECL Plus (Beyotime). Digital images were taken with by the automatic chemiluminescence imaging analysis system (Tanon).

Co-immunoprecipitation (Co-IP)

ESC extracts were prepared using lysis buffer (20 mM Tris-HCl, pH 8; 137 mM NaCl; 10% glycerol; 1% NP-40; 2 mM EDTA, supplemented with protease inhibitor and PMSF). FLAG antibody (M2) conjugated magnetic beads were washed in TBS buffer (50 mM Tris HCl, 150 mM NaCl, pH 7.4) for three times. ESC extracts were incubated with 15 μl M2 beads at 4 ℃ overnight. The immunoprecipitates were washed three times using TBS buffer, eluted in 2× SDS-PAGE loading buffer, and subjected to mass spectrometric analysis.

RNA purification and quantitative reverse-transcription PCR

Total RNA was purified using TRIZOL (Ambion) according to the manufacturer's instructions. cDNA was synthesized using Reverse Transcription Kit (Roche). PCR reactions were performed with FastStart Universal SYBR Green Master (Roche) in a Bio-Rad IQ5 system. PCR cycling conditions were 95°C for 2 min, 40 cycles of 95°C for 15 s, 58°C for 15 s, and 72°C for 30 s, and then a melting curve of the amplified DNA was acquired. Quantification of target genes was normalized with β-Actin. Primers were listed in Table S1.

RNA sequencing

Total RNA was purified using RNeasy Mini Kit (Qiagen) according to the manufacturer's instructions. Construction of RNA sequencing library, sequencing with BGISEQ-500, and bioinformatic analysis were performed by BGI Tech (Shenzhen, China). The RNA-seq data set (accession number GSE104242) has been deposited in the Gene Expression Omnibus database.

Alkaline phosphatase (AP) assay

After washing once with PBS, mouse ESCs were stained with alkaline phosphatase substrate kit Ⅲ (Vector) according to the manufacturer's instruction.

Colony forming assay

Mouse ESCs were suspended in ESC medium and cultured in a 6-well plate (800 cells per well). After 4-6 days culture, ESCs were stained for AP. The AP-positive colony were counted under microscope.

Embryoid body (EB) forming assay

Mouse ESCs were suspended in LIF free ESC medium (40,000 cells/ml) and cultured in 25 μl hanging drops. EBs were collected on day 4.

Cell cycle analysis

Cells were collected and fixed with 70% ethanol. Then stained with staining buffer (5 μg/ml propidium, 1 mg/ml RNase A) for 30 min at 37℃ and analyzed by FACSCalibur flow cytometer (BD Biosciences). Modfit software was used to analyze the results.

Apoptosis analysis

The apoptosis was detected by the Annexin V- apoptosis detection kit (Beyotime, C1067S) as recommended by the manufacturer. Cells were harvested and washed in 1×PBS once. Then resuspended in 195 μl Annexin V- EGFP binding buffer supplied with 5μl Annexin V-EGFP and 10 μl PI, incubated on RT for 20 min, and analyzed by FACSCalibur flow cytometer (BD Biosciences). Flow Jo software was used to analyze the results.

Karyotype analysis

Cells were incubated with 0.3 μg/ml nocodazole for 3-5 h to enrich cells at metaphase. These metaphase-enriched cells were harvested and exposed to 0.075 M KCl solution at 37 ℃ for 25 min. Then fixed with cold methanol: glacial acetic acid (3:1) buffer at least fourth times and spread onto clean slides. Finally, stained with DAPI for research. Cells with chromosomes more than 39 were counted.

Data processing and statistical analysis

All images were processed with Photoshop 2021 (Adobe) and Image J (National Institutes of Health). All data were analyzed using Microsoft Excel and Prism software (GraphPad Software). All experiments were confirmed with at least three independent experiments, and at

least three control or mutant embryos (the exact sample size was shown in the figure legends) were used for immunostaining. Statistical analyses were performed with χ^2, two tailed Student's *t* or two-way ANOVA test, which were indicated in the figure legends. The quantitative results were presented as the mean±SD. Statistically significant p-values were indicated in figures as *, $p < 0.05$; **, $p < 0.01$; ***, $p < 0.001$. And ns (not significant) marks p-value＞0.05.

ACKNOWLEDGMENTS

We thank the core facility at College of Life Sciences, Nankai University.

COMPETING INTERESTS

The authors declare no competing financial interests.

FUNDING

L.C. was supported by the National Key R&D Program of China (Grant No. 2021YFA1101002 and 2018YFA0107002), the National Natural Science Foundation of China (Grant No. 31871485), the Natural Science Foundation of Tianjin (Grant No. 18JCJQJC48400), the 111 Project Grant (B08011), and the Fundamental Research Funds for the Central Universities. Y.Q. was supported by the China Postdoctoral Science Foundation (Grant No. 2019M660980) and the National Natural Science Foundation of China (Grant No. 32000600).

AUTHOR CONTRIBUTIONS

Y.Q., P.N., Q.Z., X.D., X.W. Z.Y. and L.W. performed experiments, Y.Q. and P.N. analyzed the data and contributed to the paper writing, L.Y. and L.C. designed the experiments and wrote the paper.

REFERENCES

Bar-Peled, L., Schweitzer, L. D., Zoncu, R. and Sabatini, D. M. (2012). Ragulator is a GEF for the rag GTPases that signal amino acid levels to mTORC1. *Cell,* **150,** 1196-1208.

Bulut-Karslioglu, A., Biechele, S., Jin, H., Macrae, T. A., Hejna, M., Gertsenstein, M., Song, J. S. and Ramalho-Santos, M. (2016). Inhibition of mTOR induces a paused pluripotent state. *Nature,* **540,** 119-123.

Cheng, D., Liang, B. and Li, Y. (2014). HBXIP expression predicts patient prognosis in breast cancer. *Med Oncol,* **31,** 210.

Cho, S., Lee, G., Pickering, B. F., Jang, C., Park, J. H., He, L., Mathur, L., Kim, S. S., Jung, S., Tang, H. W., Monette, S., Rabinowitz, J. D., Perrimon, N., Jaffrey, S. R. and Blenis, J. (2021). mTORC1 promotes cell growth via m(6)A-dependent mRNA degradation. *Mol Cell,* **81,** 2064-2075 e2068.

Duvel, K., Yecies, J. L., Menon, S., Raman, P., Lipovsky, A. I., Souza, A. L., Triantafellow, E., Ma, Q., Gorski, R., Cleaver, S., Vander Heiden, M. G., Mackeigan, J. P., Finan, P. M., Clish, C. B., Murphy, L. O. and Manning, B. D. (2010). Activation of a metabolic gene regulatory network downstream of mTOR complex 1. *Mol Cell,* **39,** 171-183.

Fujii, R., Zhu, C., Wen, Y., Marusawa, H., Bailly-Maitre, B., Matsuzawa, S., Zhang, H., Kim, Y., Bennett, C. F., Jiang, W. and Reed, J. C. (2006). HBXIP, cellular target of hepatitis B virus oncoprotein, is a regulator of centrosome dynamics and cytokinesis. *Cancer Res,* **66,** 9099-9107.

Gangloff, Y. G., Mueller, M., Dann, S. G., Svoboda, P., Sticker, M., Spetz, J. F., Um, S. H., Brown, E. J., Cereghini, S., Thomas, G. and Kozma, S. C. (2004). Disruption of the mouse mTOR gene leads to early postimplantation lethality and prohibits embryonic stem cell development. *Mol Cell Biol,* **24,** 9508-9516.

Giguere, V. (2018). Canonical signaling and nuclear activity of mTOR-a teamwork effort to regulate metabolism and cell growth. *FEBS J,* **285,** 1572-1588.

Guertin, D. A., Stevens, D. M., Thoreen, C. C., Burds, A. A., Kalaany, N. Y., Moffat, J., Brown, M., Fitzgerald, K. J. and Sabatini, D. M. (2006). Ablation in mice of the mTORC components raptor, rictor, or mLST8 reveals that mTORC2 is required for signaling to Akt-FOXO and PKCalpha, but not S6K1. *Dev Cell,* **11,** 859-871.

Hu, N., Zhang, J., Cui, W., Kong, G., Zhang, S., Yue, L., Bai, X., Zhang, Z., Zhang, W., Zhang, X. and Ye, L. (2011). miR-520b regulates migration of breast cancer cells by targeting hepatitis B X-interacting protein and interleukin-8. *J Biol Chem,* **286,** 13714-13722.

Lakso, M., Pichel, J. G., Gorman, J. R., Sauer, B., Okamoto, Y., Lee, E., Alt, F. W. and Westphal, H. (1996). Efficient in vivo manipulation of mouse genomic sequences at the zygote stage. *Proc Natl Acad Sci U S A,* **93,** 5860-5865.

Li, H., Wang, Z., Li, Y., Fang, R., Wang, H., Shi, H., Zhang, X., Zhang, W. and Ye, L. (2018). Hepatitis B X-interacting protein promotes the formation of the insulin gene-transcribing protein complex Pdx-1/Neurod1 in animal pancreatic beta-cells. *J Biol Chem,* **293,** 2053-2065.

Li, N., Wang, Y., Che, S., Yang, Y., Piao, J., Liu, S. and Lin, Z. (2017). HBXIP over expression as an independent biomarker for cervical cancer. *Exp Mol Pathol,* **102,** 133-137.

Li, X. and Liu, S. (2016). Suppression of HBXIP Reduces Cell Proliferation, Migration and Invasion In Vitro, and Tumorigenesis In Vivo in Human Urothelial Carcinoma of the Bladder. *Cancer Biother Radiopharm,* **31,** 311-316.

Liu, B., Wang, T., Wang, H., Zhang, L., Xu, F., Fang, R., Li, L., Cai, X., Wu, Y., Zhang, W. and Ye, L. (2018). Oncoprotein HBXIP enhances HOXB13 acetylation and co-activates HOXB13 to confer tamoxifen resistance in breast cancer. *J Hematol Oncol,* **11,** 26.

Liu, F., You, X., Wang, Y., Liu, Q., Liu, Y., Zhang, S., Chen, L., Zhang, X. and Ye, L. (2014). The oncoprotein HBXIP enhances angiogenesis and growth of breast cancer through modulating FGF8 and VEGF. *Carcinogenesis,* **35,** 1144-1153.

Liu, Q., Bai, X., Li, H., Zhang, Y., Zhao, Y., Zhang, X. and Ye, L. (2013). The oncoprotein HBXIP upregulates Lin28B via activating TF II D to promote proliferation of breast cancer cells. *Int J Cancer,* **133,** 1310-1322.

Liu, S., Li, L., Zhang, Y., Zhang, Y., Zhao, Y., You, X., Lin, Z., Zhang, X. and Ye, L. (2012). The oncoprotein HBXIP uses two pathways to up-regulate S100A4 in promotion of growth and migration of breast cancer cells. *J Biol Chem,* **287,** 30228-30239.

Long, X., Lin, Y., Ortiz-Vega, S., Yonezawa, K. and Avruch, J. (2005). Rheb binds and regulates the mTOR kinase. *Curr Biol,* **15,** 702-713.

Marusawa, H., Matsuzawa, S., Welsh, K., Zou, H., Armstrong, R., Tamm, I. and Reed, J. C. (2003). HBXIP functions as a cofactor of survivin in apoptosis suppression. *EMBO J,* **22,** 2729-2740.

Melegari, M., Scaglioni, P. P. and Wands, J. R. (1998). Cloning and characterization of a novel hepatitis B virus x binding protein that inhibits viral replication. *J Virol,* **72,** 1737-1743.

Mossmann, D., Park, S. and Hall, M. N. (2018). mTOR signalling and cellular metabolism are mutual determinants in cancer. *Nat Rev Cancer,* **18,** 744-757.

Murakami, M., Ichisaka, T., Maeda, M., Oshiro, N., Hara, K., Edenhofer, F., Kiyama, H., Yonezawa, K. and Yamanaka, S. (2004). mTOR is essential for growth and proliferation in early mouse embryos and embryonic stem cells. *Mol Cell Biol,* **24,** 6710-6718.

Nada, S., Hondo, A., Kasai, A., Koike, M., Saito, K., Uchiyama, Y. and Okada, M. (2009). The novel lipid raft adaptor p18 controls endosome dynamics by anchoring the MEK-ERK pathway to late endosomes. *EMBO J,* **28,** 477-489.

Qin, Y., Zhou, Y., Shen, Z., Xu, B., Chen, M., Li, Y., Chen, M., Behrens, A., Zhou, J., Qi, X., Meng, W., Wang, Y. and Gao, F. (2019). WDR62 is involved in spindle assembly by interacting with CEP170 in spermatogenesis. *Development,* **146**.

Sancak, Y., Bar-Peled, L., Zoncu, R., Markhard, A. L., Nada, S. and Sabatini, D. M. (2010). Ragulator-Rag complex targets mTORC1 to the lysosomal surface and is necessary for its activation by amino acids. *Cell,* **141,** 290-303.

Saxton, R. A. and Sabatini, D. M. (2017). mTOR Signaling in Growth, Metabolism, and Disease. *Cell,* **168,** 960-976.

Shi, H., Fang, R., Li, Y., Li, L., Zhang, W., Wang, H., Chen, F., Zhang, S., Zhang, X. and Ye, L. (2016). The oncoprotein HBXIP suppresses gluconeogenesis through modulating PCK1 to enhance the growth of hepatoma cells. *Cancer Lett,* **382,** 147-156.

Teis, D., Taub, N., Kurzbauer, R., Hilber, D., De Araujo, M. E., Erlacher, M., Offterdinger, M., Villunger, A., Geley, S., Bohn, G., Klein, C., Hess, M. W. and Huber, L. A. (2006). p14-MP1-MEK1 signaling regulates endosomal traffic and cellular proliferation during tissue homeostasis. *J Cell Biol,* **175,** 861-868.

Villa, E., Sahu, U., O'hara, B. P., Ali, E. S., Helmin, K. A., Asara, J. M., Gao, P., Singer, B. D. and Ben-Sahra, I. (2021). mTORC1 stimulates cell growth through SAM synthesis and m(6)A mRNA-dependent control of protein synthesis. *Mol Cell,* **81,** 2076-2093 e2079.

Wang, Y., Fang, R., Cui, M., Zhang, W., Bai, X., Wang, H., Liu, B., Zhang, X. and Ye, L. (2017a). The oncoprotein HBXIP up-regulates YAP through activation of transcription factor c-Myb to promote growth of liver cancer. *Cancer Lett,* **385,** 234-242.

Wang, Y., Li, N., Che, S., Jin, T., Piao, J., Liu, S. and Lin, Z. (2017b). HBXIP suppression reduces cell proliferation and migration and its overexpression predicts poor prognosis in non-small-cell lung cancer. *Tumour Biol,* **39,** 1010428317709675.

Wang, Y., Sun, J., Li, N., Che, S., Jin, T., Liu, S. and Lin, Z. (2017c). HBXIP overexpression is correlated with the clinical features and survival outcome of ovarian cancer. *J Ovarian Res,* **10,** 26.

Wen, Y., Golubkov, V. S., Strongin, A. Y., Jiang, W. and Reed, J. C. (2008). Interaction of hepatitis B viral oncoprotein with cellular target HBXIP dysregulates centrosome dynamics and mitotic spindle formation. *J Biol Chem,* **283,** 2793-2803.

Wu, Y., Wang, X., Xu, F., Zhang, L., Wang, T., Fu, X., Jin, T., Zhang, W. and Ye, L. (2020). The regulation of acetylation and stability of HMGA2 via the HBXIP-activated Akt-PCAF pathway in promotion of esophageal squamous cell carcinoma growth. *Nucleic Acids Res,* **48,** 4858-4876.

Xu, F., You, X., Liu, F., Shen, X., Yao, Y., Ye, L. and Zhang, X. (2013). The oncoprotein HBXIP up-regulates Skp2 via activating transcription factor E2F1 to promote proliferation of breast cancer cells. *Cancer Lett,* **333,** 124-132.

Xu, F., Zhu, X., Han, T., You, X., Liu, F., Ye, L., Zhang, X., Wang, X. and Yao, Y. (2014). The oncoprotein hepatitis B X-interacting protein promotes the migration of ovarian cancer cells through the upregulation of S-phase kinase-associated protein 2 by Sp1. *Int J Oncol,* **45,** 255-263.

Yue, L., Li, L., Liu, F., Hu, N., Zhang, W., Bai, X., Li, Y., Zhang, Y., Fu, L., Zhang, X. and Ye, L. (2013). The oncoprotein HBXIP activates transcriptional coregulatory protein LMO4 via Sp1 to promote proliferation of breast cancer cells. *Carcinogenesis,* **34,** 927-935.

Zhang, W., Lu, Z., Kong, G., Gao, Y., Wang, T., Wang, Q., Cai, N., Wang, H., Liu, F., Ye, L. and Zhang, X. (2014). Hepatitis B virus X protein accelerates hepatocarcinogenesis with partner survivin through modulating miR-520b and HBXIP. *Mol Cancer,* **13,** 128.

Zhang, Y., Zhao, Y., Li, L., Shen, Y., Cai, X., Zhang, X. and Ye, L. (2013). The oncoprotein HBXIP upregulates PDGFB via activating transcription factor Sp1 to promote the proliferation of breast cancer cells. *Biochem Biophys Res Commun,* **434,** 305-310.

Zhou, X., Wang, X., Duan, J., Sun, W., Chen, Z., Li, Q., Ou, Z., Jiang, G., Ren, X. and Liu, S. (2019a). HBXIP protein overexpression predicts the poor prognosis of pancreatic ductal adenocarcinomas. *Pathol Res Pract,* **215,** 343-346.

Zhou, X. L., Zhu, C. Y., Wu, Z. G., Guo, X. and Zou, W. (2019b). The oncoprotein HBXIP competitively binds KEAP1 to activate NRF2 and enhance breast cancer cell growth and metastasis. *Oncogene,* **38,** 4028-4046.

Zhou, Y., Qin, Y., Qin, Y., Xu, B., Guo, T., Ke, H., Chen, M., Zhang, L., Han, F., Li, Y., Chen, M., Behrens, A., Wang, Y., Xu, Z., Chen, Z. J. and Gao, F. (2018). Wdr62 is involved in female meiotic initiation via activating JNK signaling and associated with POI in humans. *PLoS Genet,* **14,** e1007463.

Zou, W., Ma, X., Yang, H., Hua, W., Chen, B. and Cai, G. (2017). Hepatitis B X-interacting protein promotes cisplatin resistance and regulates CD147 via Sp1 in ovarian cancer. *Exp Biol Med (Maywood),* **242,** 497-504.

Figures

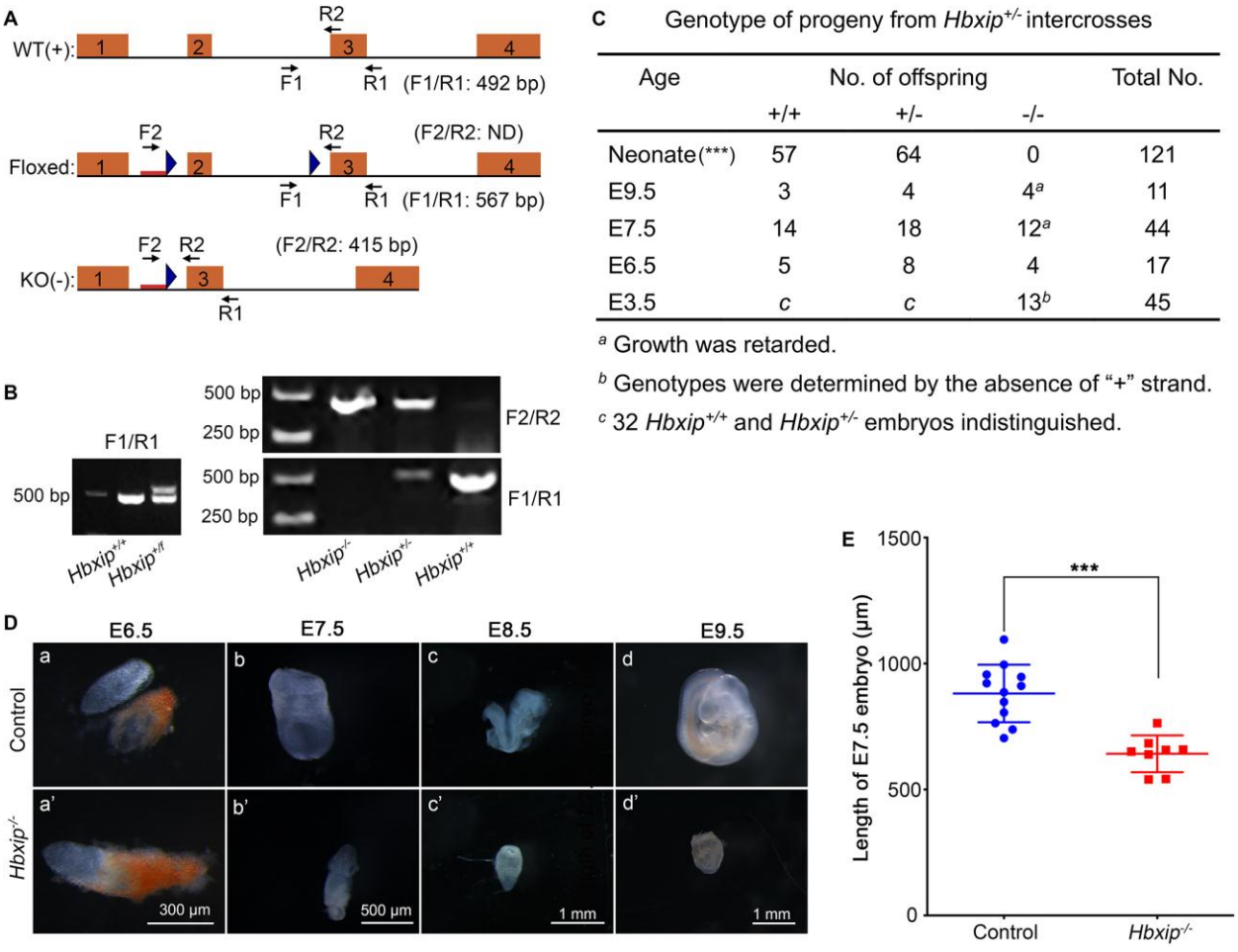

C Genotype of progeny from *Hbxip*$^{+/-}$ intercrosses

Age	No. of offspring			Total No.
	+/+	+/-	-/-	
Neonate(***)	57	64	0	121
E9.5	3	4	4[a]	11
E7.5	14	18	12[a]	44
E6.5	5	8	4	17
E3.5	*c*	*c*	13[b]	45

[a] Growth was retarded.

[b] Genotypes were determined by the absence of "+" strand.

[c] 32 *Hbxip*$^{+/+}$ and *Hbxip*$^{+/-}$ embryos indistinguished.

Fig. 1. Embryonic lethality in *Hbxip*$^{-/-}$ mice.

(A) Schematic illustration of WT, floxed, and KO alleles of *Hbxip*. Orange rectangles represent *Hbxip* exons, and blue triangles marks loxP sequences. Red bars in the floxed and KO alleles are the exogenous DNA fragment from the targeting vector. Arrows show the primers for genotyping PCR. (B) Representative genotyping PCR results. (C) Genotyping of E3.5, E6.5, E7.5, E9.5 embryos and neonate mice derived from the intercrossing of *Hbxip*$^{+/-}$ mice. χ^2 test was performed on the number of mouse mutants obtained per stage in comparison to the expected Mendelian ratios. ***, $p < 0.001$. (D) The morphology of dissected control (including WT and *Hbxip*$^{+/-}$) and *Hbxip*$^{-/-}$ embryos, without any staining, at various stages. (a) E6.5 Control, n=13; (a') E6.5 *Hbxip*$^{-/-}$, n=4; (b) E7.5 Control, n=12; (b') E7.5 *Hbxip*$^{-/-}$, n=8; (c) E8.5 Control,

n=8; (c') E8.5 *Hbxip*$^{-/-}$, n=6; (d) E9.5 Control, n=7; (d') E9.5 *Hbxip*$^{-/-}$, n=4. Scale bars: 300 μm (a, a'), 500 μm (b, b'), 1 mm (c, c', d, d'). (E) Quantification of the length of E7.5 *Hbxip*$^{-/-}$ and control (including WT and *Hbxip*$^{+/-}$) embryos. Data are shown as mean ± SD. Control, n=12; *Hbxip*$^{-/-}$, n=8. Statistical analysis was performed with two tailed Student's *t* test. ***, $p < 0.001$.

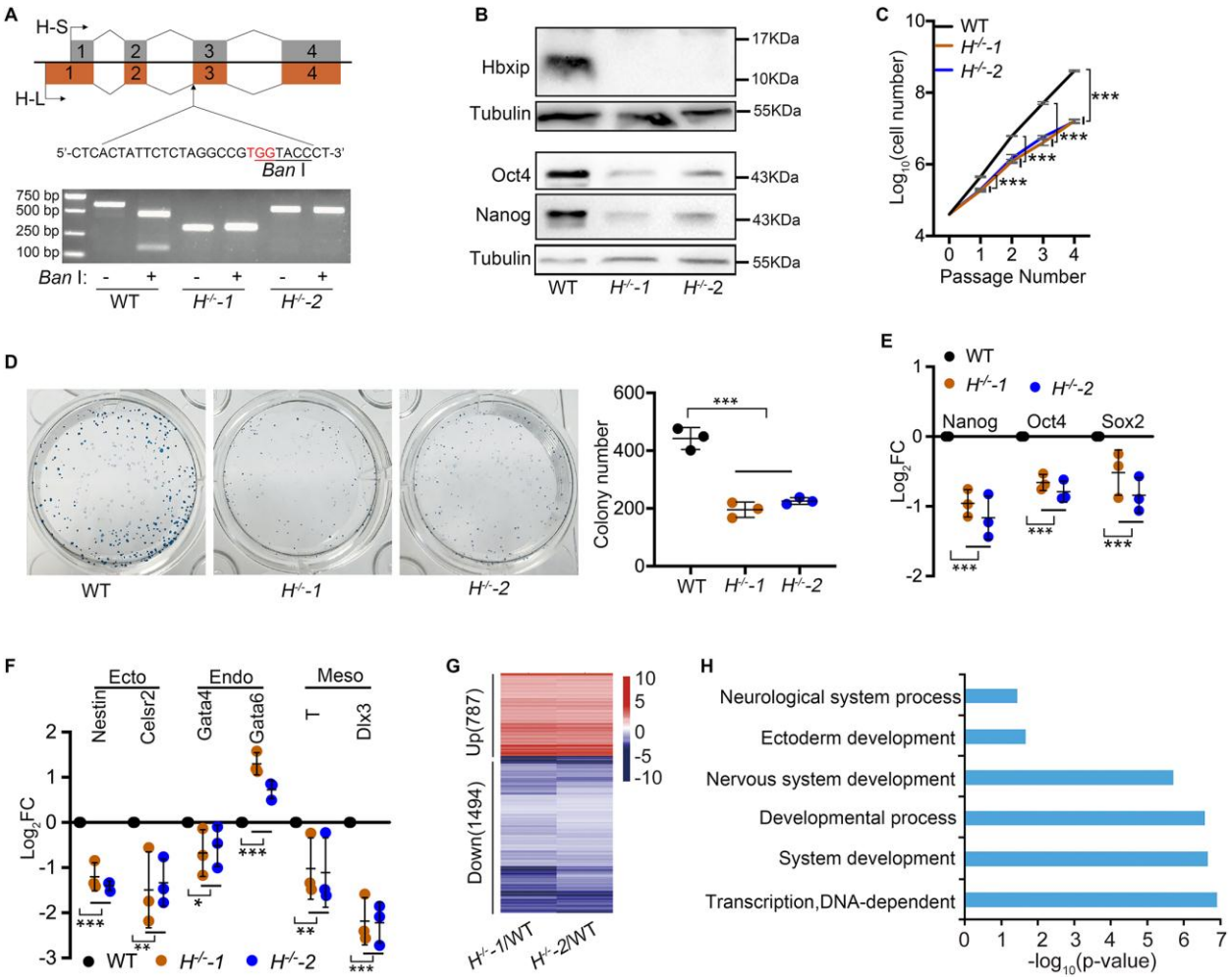

Fig. 2. Compromised self-renewal of *Hbxip*$^{-/-}$ ESCs.

(A) Schematic illustration of the strategy for knocking out *Hbxip* in ESCs. The exons of two *Hbxip* isoforms, H-S and H-L, are represented by grey and orange rectangles, respectively. The targeting sequence of sgRNA is shown. The protospacer-adjacent motif (PAM) is highlighted in red, and the *Ban* I site is underlined. The bottom panel shows the validation of *Hbxip* KO in two independent ESC clones by PCR and *Ban* I digestion. (B) Western blots show that the levels of pluripotency factors Nanog and Oct4 are reduced in *Hbxip*$^{-/-}$ ESCs. (C) Growth curves of WT and *Hbxip*$^{-/-}$ ESCs. (D) Colony forming assay of WT and *Hbxip*$^{-/-}$ ESCs. The left panel shows representative AP staining images of colony forming assays. The right panel is the quantification results of three repeated colony forming assays. (E) The expression of pluripotency genes *Nanog*, *Oct4*, and *Sox2* in WT and *Hbxip*$^{-/-}$ ESCs, measured by quantitative RT-PCR. Fold change (FC) was calculated by comparing to WT ESCs. (F) The expression of differentiation genes in WT

and *Hbxip*$^{-/-}$ ESCs. FC was calculated by comparing to WT ESCs. (G) The heatmap showing the differentially expressed genes in *H*$^{-/-}$-1 and *H*$^{-/-}$-2 ESCs, compared to WT ESCs, detected by RNA-seq. (H) GO annotation of the downregulated genes in *Hbxip*$^{-/-}$ ESCs. For growth curve, colony formation, quantitative RT-PCR and Western blot, n=3. Data are shown as mean ± SD. Statistical analysis was performed with two-way ANOVA test. *, $p < 0.05$; **, $p < 0.01$; ***, $p < 0.001$.

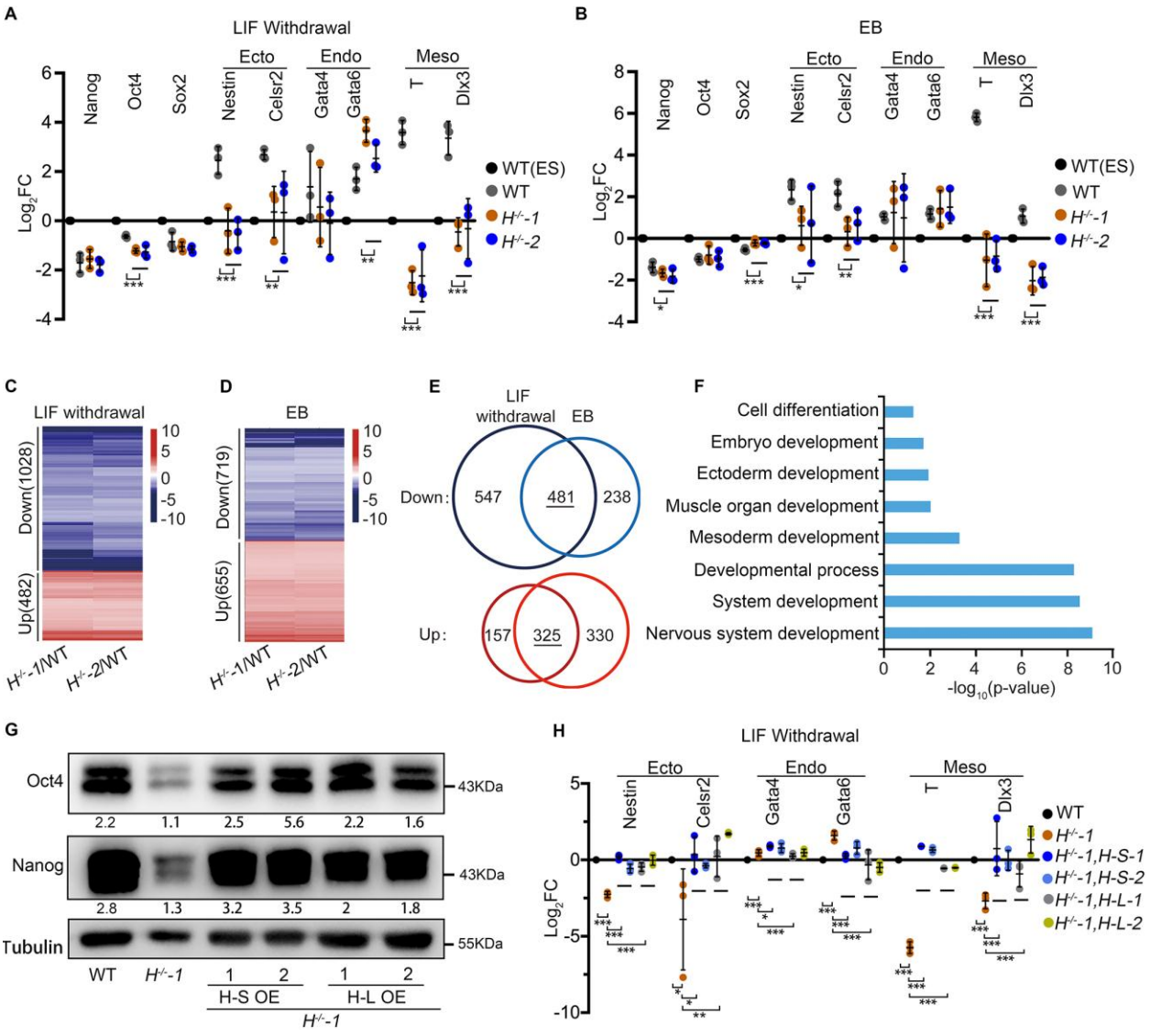

Fig. 3. Differentiation defects of *Hbxip*$^{-/-}$ ESCs.

(A) and (B) The expression of differentiation genes in differentiated WT and *Hbxip*$^{-/-}$ ESCs by LIF-withdrawal for 4 days (A) and in day 4 WT and *Hbxip*$^{-/-}$ EBs (B). FC was calculated by comparing to undifferentiated WT ESCs, marked as WT(ES). (C) and (D) The heatmaps show the differentially expressed genes in differentiated *Hbxip*$^{-/-}$ ESCs by LIF-withdrawal for 4 days (C) and day 4 *Hbxip*$^{-/-}$ EBs (D), compared to their WT counterparts, detected by RNA-seq. (E) Venn diagrams show the commonly regulated genes (481 downregulated and 325 upregulated genes) by *Hbxip* KO in two differentiation protocols, LIF-withdrawal and EB differentiation. (F) GO annotation of the commonly downregulated genes by *Hbxip* KO. (G) Overexpression of

Hbxip, both H-L and H-S, rescues the expression levels of Nanog and Oct4 proteins in *Hbxip* KO ESCs. The quantified levels of Nanog and Oct4 were shown below the corresponding blots. (H) Overexpression of *Hbxip*, both H-L and H-S, rescues the expression levels of differentiation genes in differentiated *Hbxip* KO ESCs by LIF-withdrawal for 4 days. FC was calculated by comparing to differentiated WT ESCs. For quantitative RT-PCR and Western blot, n=3. Data are shown as mean ± SD. Statistical analysis was performed with two-way ANOVA test. *, $p < 0.05$; **, $p < 0.01$; ***, $p < 0.001$.

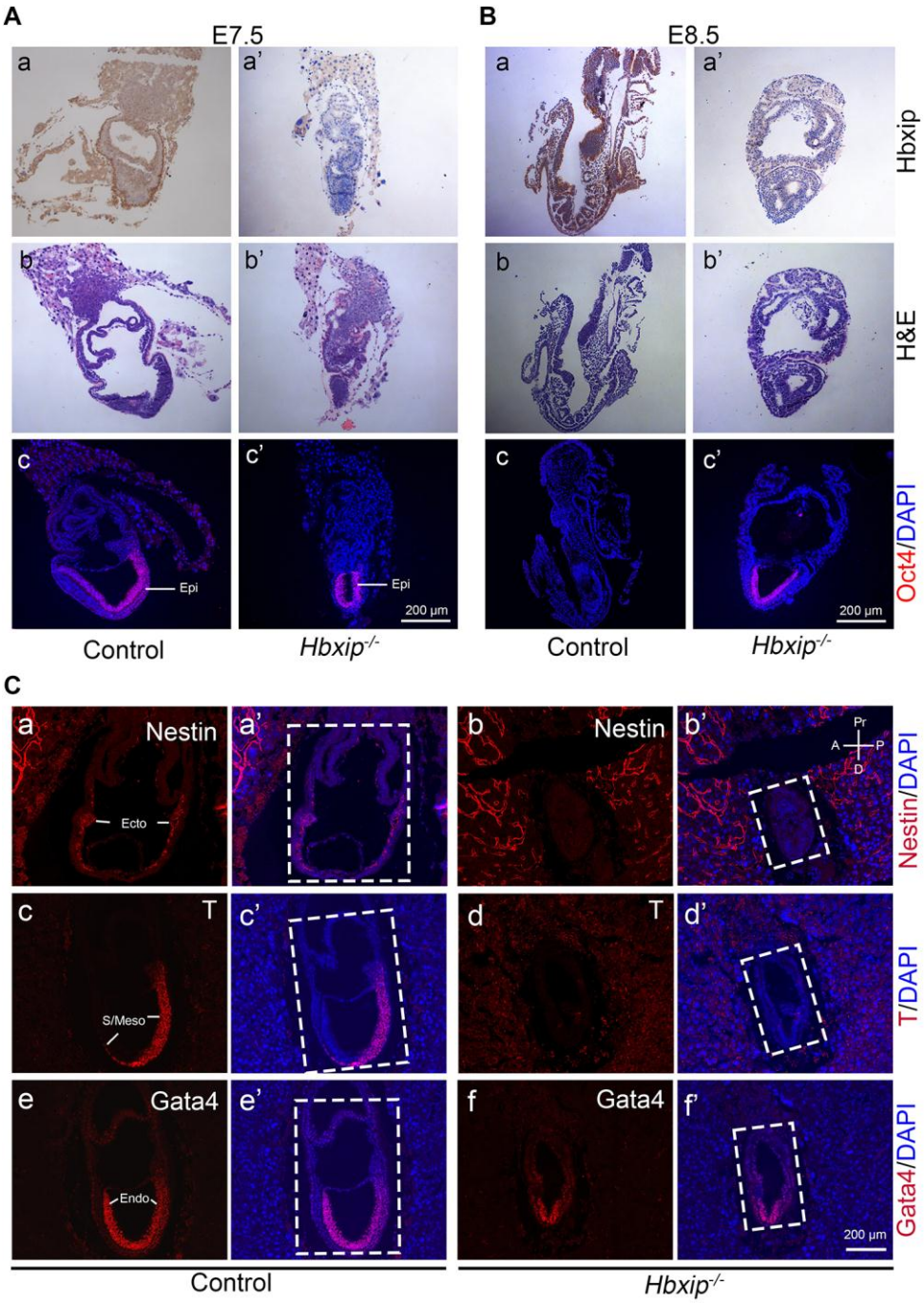

Fig. 4. Defective epiblast proliferation and differentiation in *Hbxip*$^{-/-}$ embryos.

(A) and (B) Control and *Hbxip*$^{-/-}$ E7.5 (A) and E8.5 (B) embryo sections were subjected to immunohistochemistry staining for Hbxip (a and a'), H&E staining (b and b'), and immunofluorescence staining for Oct4 (c and c'). Epi: epiblast. E7.5 (Control, n=14; *Hbxip*$^{-/-}$, n=8); E8.5 (Control, n=8; *Hbxip*$^{-/-}$, n=5). (C) Immunofluorescence staining of control (n=7) and

Hbxip$^{-/-}$ (n=3) E7.5 embryo sections for Nestin (a, a', b, b'), T (c, c', d, d'), and Gata4 (e, e', f, f') revealed ectodermal and mesodermal defects in *Hbxip*$^{-/-}$ embryos. Control embryos include WT and *Hbxip*$^{+/-}$ embryos. Dashed rectangles mark the embryo part. Ecto: Ectoderm, S/Meso: Streak/Mesoderm, Endo: Endoderm. Scale bars: 200 μm.

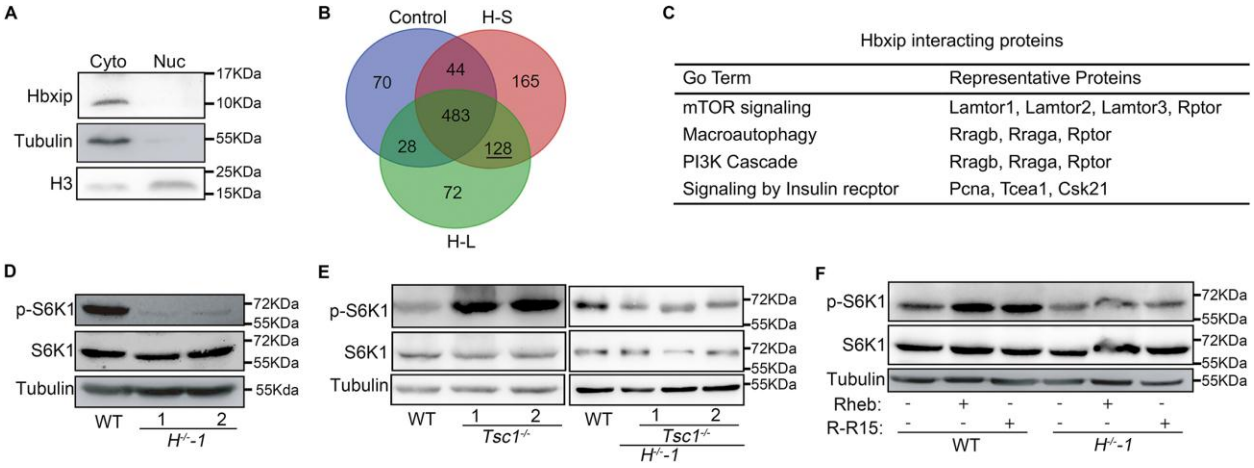

Fig. 5. Hbxip is required for mTORC1 activation.

(A) Western blot analysis of Hbxip in the cytoplasmic and nuclear fractions of ESCs. (B) Venn diagram of proteins identified by mass spectrometric analysis. Co-IP experiments were performed with cell extracts from ESCs expressing FLAG-Hbxip (H-L and H-S) and control ESCs with empty vector, using M2 magnetic beads. The resulting IP samples were analyzed by mass spectrometry. 128 proteins identified in both the H-L and H-S samples, but not in the control, are called as Hbxip interacting proteins. (C) GO annotation of the 128 Hbxip-interacting proteins. (D) Western blots of S6K1 and p-S6K1 in WT and *Hbxip*$^{-/-}$ ESCs demonstrate the reduced mTORC1 activity in *Hbxip*$^{-/-}$ ESCs. (E) Western blots of S6K1 and p-S6K1 in WT, *Tsc1*$^{-/-}$, *H*$^{-/-}$-1, and *Tsc1*$^{-/-}$; *H*$^{-/-}$-1 ESCs show that *Tsc1* KO fails to activate mTORC1 in *Hbxip*$^{-/-}$ ESCs. (F) Overexpression of Rheb or Rptor fused with the lysosome-targeting signal of Rheb (R-R15) is unable to activate mTORC1 in *Hbxip*$^{-/-}$ ESCs. WT and *H*$^{-/-}$-1 ESCs were transfected with empty vector, or plasmids expressing Rheb or R-R15. Two days after transfection, ESCs were harvested for Western blot analysis. For Western blot, n=3.

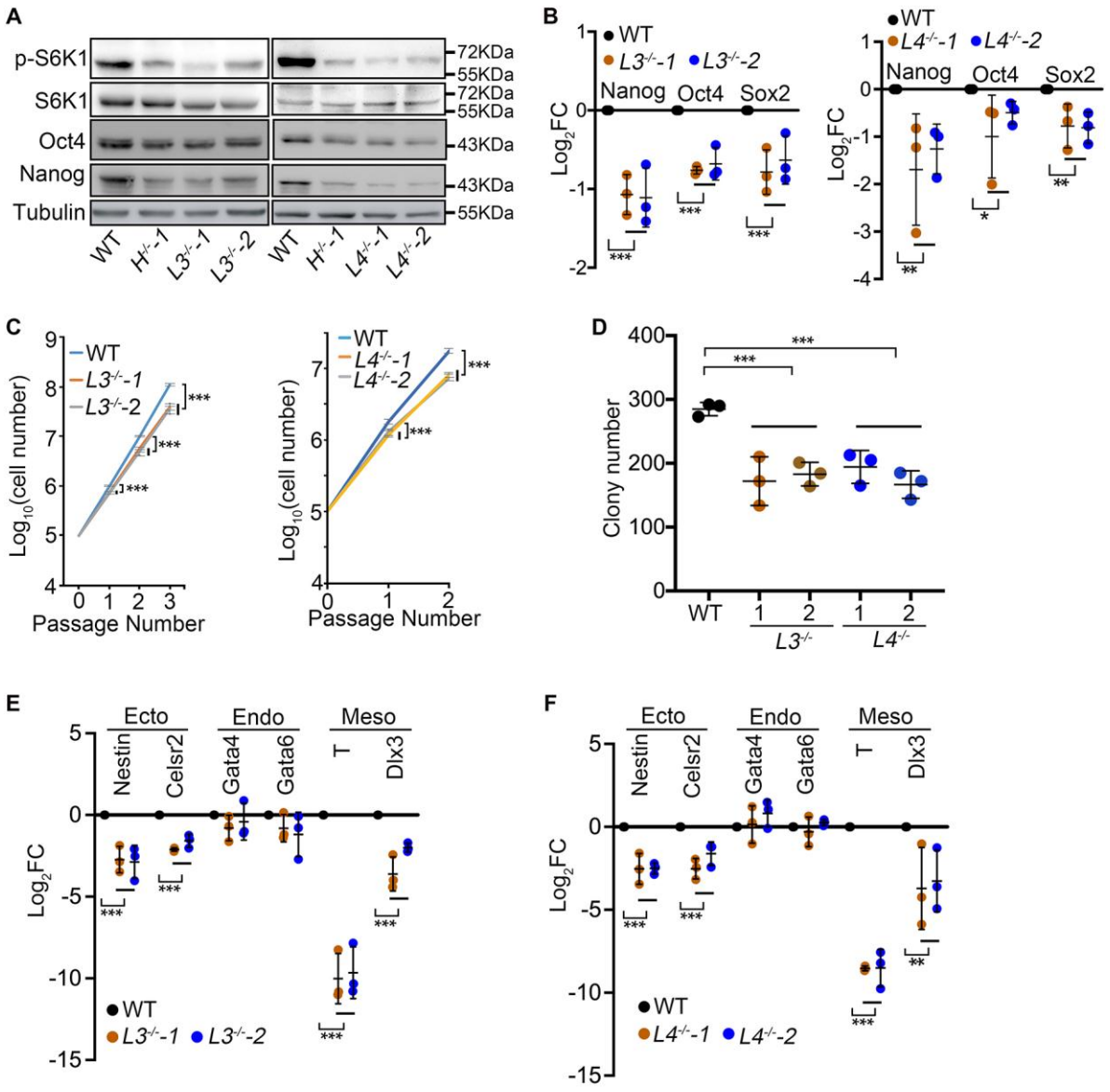

Fig. 6. Differentiation defects in ESCs lacking other Ragulator subunits.

(A) Western blots of S6K1, p-S6K1, Nanog, and Oct4 in WT, *Hbxip*$^{-/-}$, *Lamtor3*$^{-/-}$ (*L3*$^{-/-}$) and *Lamtor4*$^{-/-}$ (*L4*$^{-/-}$) ESCs. (B) The expression levels of pluripotency genes in WT, *L3*$^{-/-}$ and *L4*$^{-/-}$ ESCs measured by quantitative RT-PCR. FC was calculated by comparing to WT ESCs. (C) Growth curves of WT, *L3*$^{-/-}$ and *L4*$^{-/-}$ ESCs. (D) Colony forming assays of WT, *L3*$^{-/-}$ and *L4*$^{-/-}$ ESCs. (E) and (F) The expression levels of differentiation genes in differentiated WT, *L3*$^{-/-}$ (E) and *L4*$^{-/-}$ (F) ESCs. ESCs were differentiated for 96 hours in the absence of LIF. The resulting differentiated cells were harvested for quantitative RT-PCR. FC was calculated by comparing to

differentiated WT ESCs. For growth curve, colony formation, quantitative RT-PCR and Western Blots, n=3. Data are shown as mean ± SD. Statistical analysis was performed with two-way ANOVA test. *, $p < 0.05$; **, $p < 0.01$; ***, $p < 0.001$.

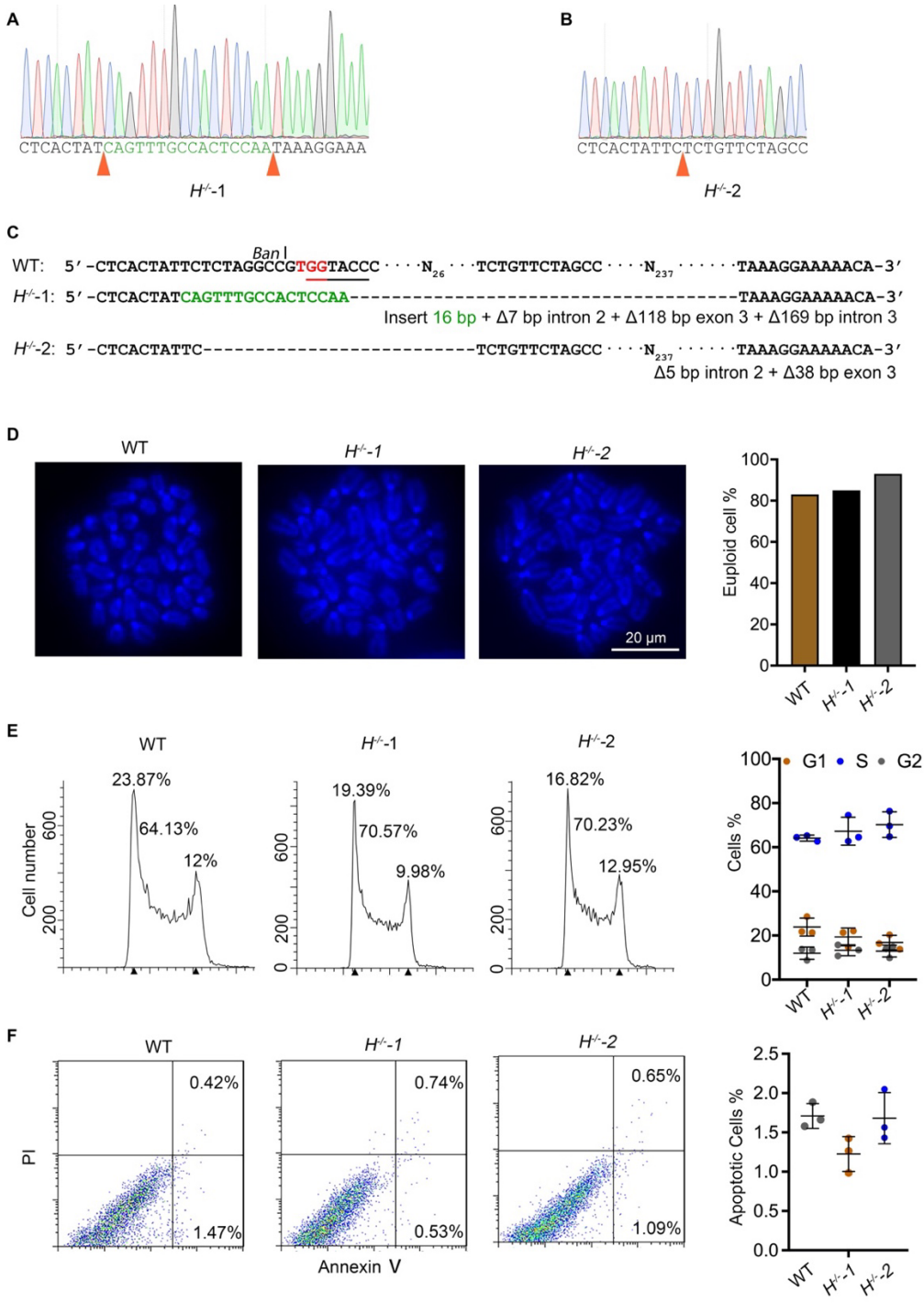

Fig. S1. Related to Fig. 2. Validation of *Hbxip*$^{-/-}$ ESC clones.

(A) and (B) Sequencing chromatograph of the *Hbxip* gene around the Cas9 targeting site in *H*$^{-/-}$-1 (A) and *H*$^{-/-}$-2 (B) ESCs. Orange triangles mark the indel mutations introduced by Cas9 cutting. (C) Sequence alignment of the *Hbxip* gene around the Cas9 targeting site in WT, *H*$^{-/-}$-1 and *H*$^{-/-}$-2 ESCs. (D-F) Karyotyping (D), cell cycle (E), and apoptosis (F) analyses of WT and *Hbxip*$^{-/-}$ ESCs. (D) More than 30 metaphase spreads were counted for each cell line. Scale bar: 20 μm. (E) and (F) For cell cycle and apoptosis analyses, data are shown as mean ± SD (n=3). Statistical analysis was performed with two-way ANOVA test. $p > 0.05$ was considered as statistical non-significance.

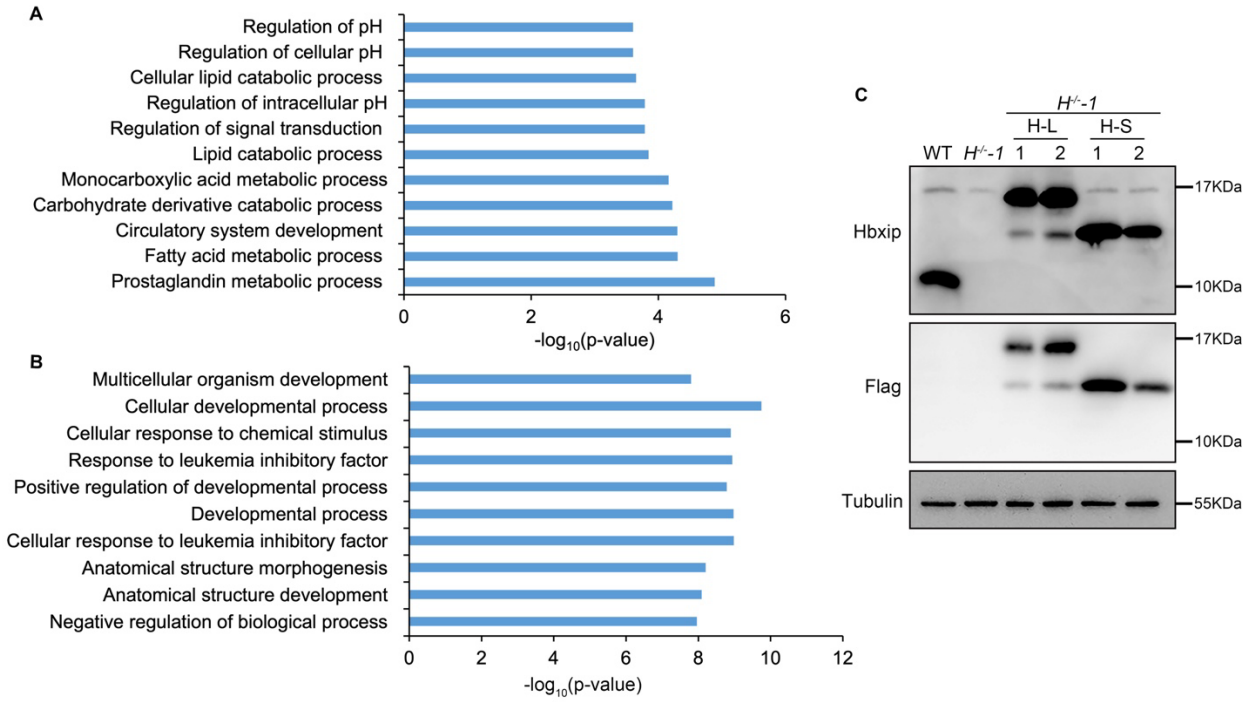

Fig. S2. Related to Figs 2, 3. *Hbxip KO* affects gene expression and mTORC1 activity.
(A) GO annotation of the upregulated genes in *Hbxip*$^{-/-}$ ESCs (Related to Fig. 2G, H). (B) GO annotation of the commonly upregulated genes by *Hbxip* KO (Related to Fig. 3C-F). (C) Validation of the overexpression of Flag tagged Hbxip, including H-L and H-S (Related to Fig. 3G).

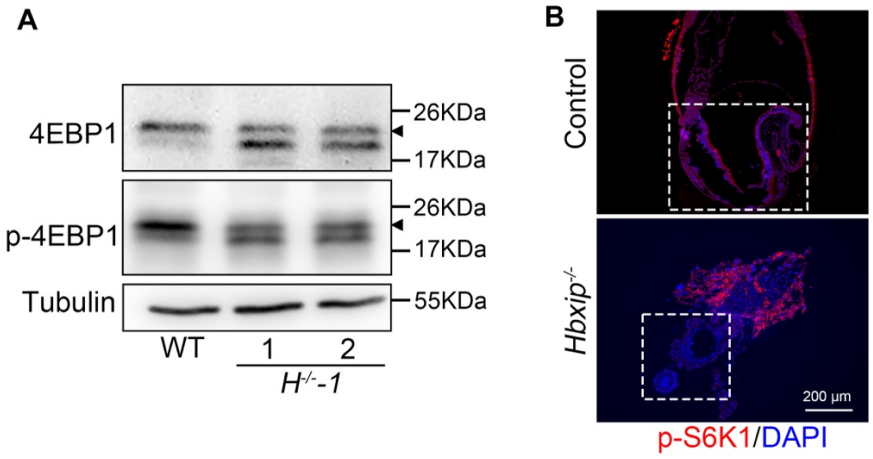

Fig. S3. Related to Fig. 5. Reduced mTOCRC1 activity in *Hbxip*$^{-/-}$ ESCs and embryos.
(A) Western blots of 4EBP1 and p-4EBP1 in WT and *Hbxip*$^{-/-}$ ESCs demonstrate the reduced mTORC1 activity in *Hbxip*$^{-/-}$ ESCs. Triangles mark the specific bands for 4EBP1 and p-4EBP1. (B) Immunofluorescence staining of p-S6K1 in control and *Hbxip*$^{-/-}$ E8.5 embryo sections. Dashed rectangles mark the embryo part. Control (including WT and *Hbxip*$^{+/-}$), n=4; *Hbxip*$^{-/-}$, n=4. Scale bar: 200 μm.

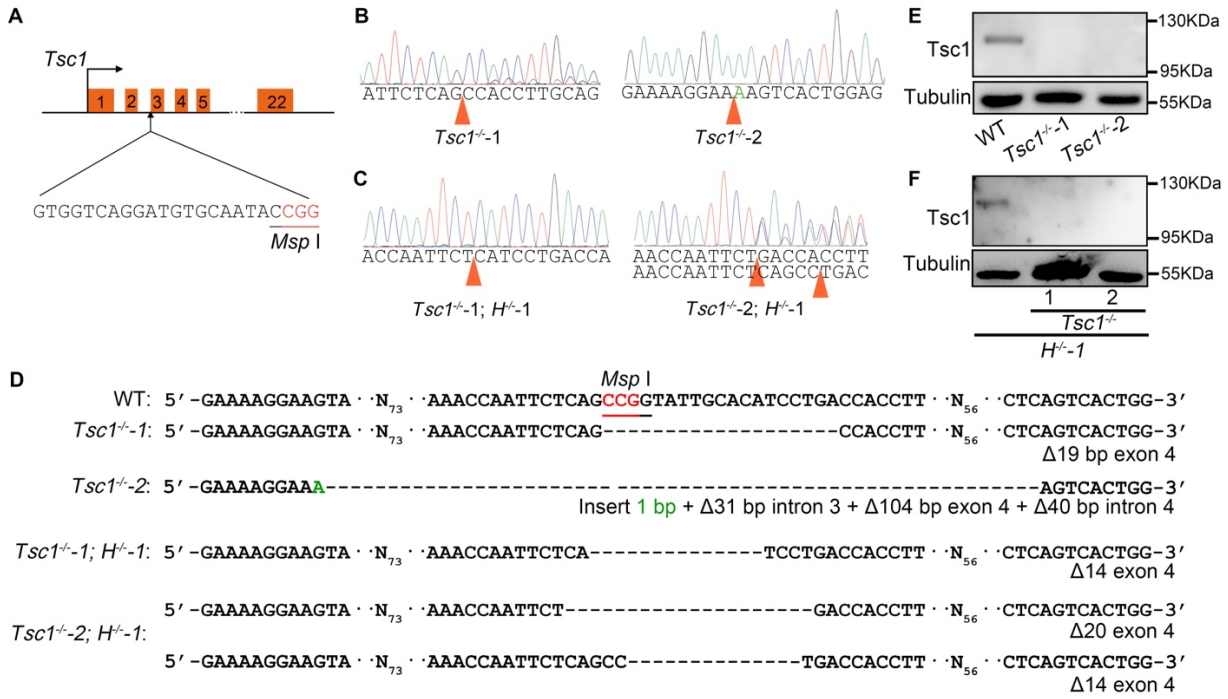

Fig. S4. Related to Fig. 5. Validation of *Tsc1*$^{-/-}$ ESC clones.

(A) Schematic illustration of the strategy for knocking out *Tsc1* in ESCs. The targeting sequence of sgRNA is shown. The protospacer-adjacent motif (PAM) is highlighted in red, and the *Msp* I site is underlined. (B) and (C) Sequencing chromatograph of the *Tsc1* gene around the Cas9 targeting site in *Tsc1*$^{-/-}$ (B) and *Tsc1*$^{-/-}$; *H*$^{-/-}$-1 (C) ESCs. Orange triangles mark the indel mutations introduced by Cas9 cutting. (D) Sequence alignment of the *Tsc1* gene around the Cas9 targeting site in WT, *Tsc1*$^{-/-}$ and *Tsc1*$^{-/-}$; *H*$^{-/-}$-1 ESCs. (E) and (F) Validation of Tsc1 knockout in *Tsc1*$^{-/-}$ (E) and *Tsc1*$^{-/-}$; *H*$^{-/-}$-1 (F) ESCs by Western blot.

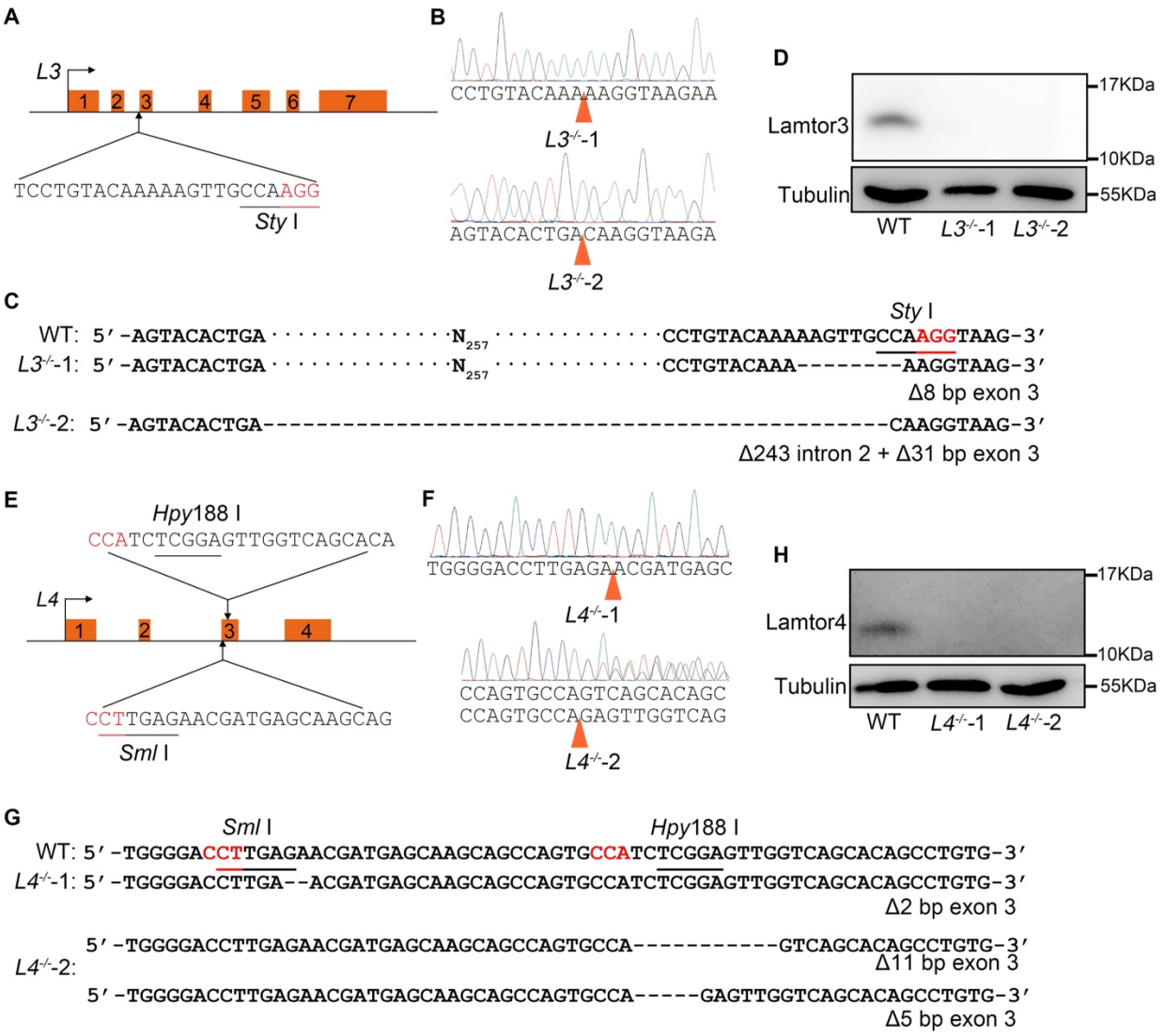

Fig. S5. Related to Fig. 6. Validation of *Lamtor3*$^{-/-}$ and *Lamtor4*$^{-/-}$ ESC clones.

(A) and (E) Schematic illustration of the strategy for knocking out *Lamtor3* (A) and *Lamtor4* (E) in ESCs. The targeting sequences of sgRNAs (one for *Lamtor3* and two for *Lamtor4*) are shown. The protospacer-adjacent motif (PAM) is highlighted in red, and the *Sty* I, *Sml* I and *Spy*188 I sites are underlined. (B) and (F) Sequencing chromatograph of the *Lamtor3* and *Lamtor4* gene around the Cas9 targeting site in *Lamtor3*$^{-/-}$ (B) and *Lamtor4*$^{-/-}$ (F) ESC clones. Orange triangles mark the indel mutations introduced by Cas9 cutting. (C) and (G) Sequence alignment of the *Lamtor3* (C) and *Lamtor4* (G) gene around the Cas9 targeting site in WT, *Lamtor3*$^{-/-}$ (C) and *Lamtor4*$^{-/-}$ (G) ESCs. (D) and (H) Validation of Lamtor3 (D) and Lamtor4 (H) knockout in *Lamtor3*$^{-/-}$ (D) and *Lamtor4*$^{-/-}$ (H) ESCs by Western blot.

Table S1. Primers for quantitative RT-PCR

Gene	Forward	Reverse
Nanog	TACAAGGGTCTGCTACTGAGATGC	TTGGGACTGGTAGAAGAATCAGGG
Oct4	ATCAGCTTGGGCTAGAGAAGGATG	AAAGGTGTCCCTGTAGCCTCATAC
Sox2	GCGGAGTGGAAACTTTTGTCC	CGGGAAGCGTGTACTTATCCTT
Nestin	CTGGATCTGGAAGTCAACAGAGGT	ATCCTCAGTTTCCACTCCTGTAGC
Gata4	GCTATGCATCTCCTGTCACTCAGA	CCAAGTCCGAGCAGGAATTTGAAG
Gata6	CTTCTCCTTCTACACAAGCGACCA	ATACTTGAGGTCACTGTTCTCGGG
T	CATCGGAACAGCTCTCCAACCTAT	TACCATTGCTCACAGACCAGAGAC
Celsr2	CACGATGGCCTGAGGGTTT	CCTTGTGGAGAAAGGTGTCCT
Dlx3	CACTGACCTGGGCTATTACAGC	GAGATTGAACTGGTGGTGGTAG
β-Actin	CAGAAGGAGATTACTGCTCTGGCT	TACTCCTGCTTGCTGATCCACATC

Table S2. Differentially expressed genes (DEGs) identified in *Hbxip*$^{-/-}$ ESCs, compared to WT ESCs.

Click here to download Table S2

Table S3. DEGs identified in differentiated *Hbxip*$^{-/-}$ ESCs, compared to differentiated WT ESCs.

WT, *H*$^{-/-}$-1, and *H*$^{-/-}$-2 ESCs were differentiated for 4 days by two methods, LIF withdrawal and EB. RNA purified from these differentiated cells were subjected to RNA-seq analysis.

Click here to download Table S3

Table S4. Hbxip interacting proteins identified by co-IP and mass spectrometry.

Click here to download Table S4